Reverse Magnus Force on a Magnetically Suspended Ogive Cylinder at Subsonic Speeds

E. P. Birtwell,* J. B. Coffin,† E. E. Covert,‡ and C. W. Haldeman§
Massachusetts Institute of Technology, Cambridge, Mass.

Data are presented showing an additional domain of reversed sign Magnus force coefficient. This phenomenon was found in essentially incompressible flow in a length Reynolds number range of at least 0.77×10^6-1.1×10^6 and for an angle of attack range of 0 to ± 4.5 deg. Furthermore the location of the center of pressure is independent of the sign of the Magnus force coefficient. Finally, the presence of a dummy sting support system and an artificially induced turbulent boundary layer causes the reversed sign region to vanish for all practical purposes.

Nomenclature

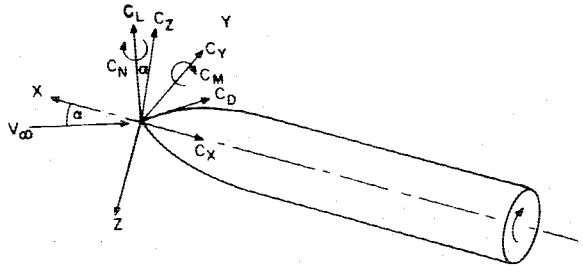

C_D = drag coefficient, drag/qS
C_L = lift coefficient, lift/qS
C_M = pitching-moment coefficient (about nose) = pitching moment/qSL
C_{M_α} = pitching-moment slope
C_N = Magnus yawing moment coefficient (about nose) = yawing moment/qSL¶
C_{NP} = linear Magnus moment coefficient, $C_N/(PD/2V_\infty)$
C_X = axial force coefficient
C_Y = Magnus side force coefficient, side force/qS¶
C_{YP} = linear Magnus force coefficient, $C_Y/(PD/2V_\infty)$
C_Z = normal force coefficient
C_{Z_α} = normal force coefficient slope
D = model diameter
L = model length
M = Mach number
P = spin rate, rad/s
q = dynamic pressure
Re_L = Reynolds number based on model length
S = model base area
V_0 = steady component of velocity
V_∞ = freestream velocity
ΔV = fluctuating component of velocity
x = axial position
x_{cp}, CP = center of pressure location diameters from the nose
α = angle of attack
Δ = standard deviation

Received Nov. 11, 1976; revision received Oct. 25, 1977.

Index categories: Aerodynamics; Ground Testing; Subsonic Flow.

*Research Assistant, Department of Aeronautics and Astronautics, Aerophysics Laboratory. Present address: General Electric Company, Lynn, Mass.

†Research Engineer, Francis Bitter National Magnet Laboratory.

‡Professor of Aeronautics and Astronautics, Department of Aeronautics and Astronautics, Aerophysics Laboratory. Fellow, AIAA.

§Research Associate, Department of Aeronautics and Astronautics, Aerophysics Laboratory. Member AIAA.

¶No spin tare subtracted.

Introduction

CONSIDER a slender, spinning body of revolution with the origin of a coordinate system located at the center of volume. The x axis is positive forward and is coincident with the axis of revolution. The y and z axes form a right-handed set. A positive spin about the x axis is defined by the right-hand rule. Both the velocity vector and the vertical lie in the x, z plane. Angle of attack is the angle between the velocity vector and the x axis, positive nose up. The aerodynamic forces acting on this spinning body, when it it at a positive angle of attack, consist of a normal force in the negative z direction, an axial force in the negative x direction, and under most circumstances a side force acting in the negative y direction. This latter force is called the Magnus force. If the spin is positive, a reversed Magnus force acts in the positive y direction. Two classes of reversed Magnus force have been reported. First, measurements of the reverse Magnus force have been reported at moderate angles of attack by Fletcher.[1] He has shown that this reversed Magnus force occurs because of an interaction between the shed vorticity due to lift and the asymmetrical spin-induced boundary-layer transition. This criterion causes the azimuthal origin of the feeding sheet to become asymmetrically disposed.** A second class of reversed Magnus force has been measured by Martin[2] and Birtwell.[3] This reversed Magnus force occurs at small values of angle of attack. A model that explains the origin of the second class of reversed Magnus force has yet to be published.

While it is reasonable to assume that the second class of reversed Magnus force is also due to asymmetric boundary-layer transition, this conjecture remains to be proved. The data presented below show that reversed Magnus force exists in the Reynolds number regime when it is possible for spin-induced asymmetric boundary-layer transition to occur. However, the reverse Magnus force also exists when the boundary layer is fully turbulent downstream of a boundary-layer trip. The data also show that the presence of a sting reduces the size of the reversed Magnus force markedly.

Description of Experiment

The experimental results were obtained at low subsonic speeds ($M \leq 0.43$). Since the model, a 5-caliber tangent ogive

**This class of reversed Magnus force seems to be related to the same kind of phenomena that caused the reversed Magnus force to appear on two-dimensional flow past a spinning cylinder. See Krahn[4] and Swanson[5] for a more detailed discussion of the phenomena.

cylinder, was magnetically suspended, the aerodynamic interference between the suspension system and the model was negligible. The magnetic balance and low turbulence tunnel have been described in detail elsewhere.[3,6]

Flow quality in the 32-in.-long test section was determined by rake surveys at the inlet (station − 16 in.) and exit (station + 16 in.), indicating a dynamic pressure variation across the 4-in.-diam central core within 0.2% of the mean dynamic pressure.[6] The axial variation of the mean dynamic pressure is a decrease of 2.0% along the 32-in. test section at maximum dynamic pressure. If q is determined by its value at the model center, this gradient corresponds to a $\pm 0.15\%$ change over the length of the model and is not significant compared to the $\pm 0.3\%$ uncertainty in C_Y from other sources.

The turbulence level ($0.707\sqrt{\Delta V^2/V_0^2}$) in the test section was measured using a transverse hot wire[6] and was found to be 0.07% at $Re_L = 420{,}000$ and 0.26% at $Re_L = 790{,}000$ based on the length of the present model. This level, which is typical of 1960 vintage subsonic tunnels, is sufficiently low that boundary layers on the test section walls are laminar and drag data on spheres[7] do not exhibit natural transition at $Re = 310{,}000$.

A laser angle-of-attack and angle-of-yaw measuring and control system held the angles of attack and yaw within 0.02 deg (Ref. 8) once it was engaged. The absolute position of zero angle of attack was, however, uncertain within approximately ± 0.15 deg as a result of mechanical assembly of the test section and balance and viewing accuracy through the transits.

The model has a frontal blockage area of 2.25% and the standard corrections were made for solid and wake blockage. Earlier measurements of the drag of ellipsoids in this tunnel[9] indicate that these corrections are adequate to collapse the data for blockages of 0.3% to 3%. References 9 and 16 as well as the present drag data suggest that the effect of spin on bounday-layer transition is stronger than the effect of a possible 25% reduction in model size, which would produce negligible blockage effects on the aerodynamic coefficients.

The length Reynolds number runs from 7×10^5-1.26×10^6. Thus, the boundary-layer flow is in a transition region. Roughness was added to the surface to insure turbulent boundary layers when needed. The spin rates or velocity ratios are of the order of 0.2 or less.

The model rolling motion was generated by superimposing a two-phase, 1200-Hz. a.c. electromagnetic field on the d.c. fields used for pitch and yaw control. Interference from this 4-kW, 1200-Hz field was eliminated by recording data as the model spin decayed from its peak value after turning off the roll-driving field.

Data Acquisition

Force data from the magnetic balance were read out as voltage signals from shunts in the several coil circuits. In addition, an output signal proportional to model spin was developed by a photocell mounted in a transit. An image of the model afterbody, which was painted with 10 black stripes, was focused on the photocell. The output pulses, counted for 0.1 s, thus gave the model spin rate in rps.

These signals for lift, side force, drag, pitch, yaw magnetizing current, and spin along with dynamic pressure were recorded with an integrating digital voltmeter and a digital recorder while being scanned sequentially. Spin rate was recorded at the beginning and end of the data print cycle, the variation being typically less than 3 rps over the 2-s period of scanning cycle.

The pressure across the wind tunnel expansion section was measured with a micromanometer to 0.0003 psi and was used to determine test-section dynamic pressure. This reading was used periodically to check less accurate transducer readings that were printed with other data.

Balance Calibration

The force-current relations used for balance calibration are described by Birtwell.[3] These were linearized for small angles of attack as described by Gilliam.[10] Both the force calibration constants and the angle moment interaction for pitch and yaw were determined experimentally for each model tested following Gilliam.

Models

Two boundary-layer trip configurations and the clean tangent-ogive nose cylinder are shown in Fig. 1. The models were machined from electrolytic ingot iron and weighed approximately 1 lb each. Either #180 carborundum grit or a 0.012-in.-square cross-section trip ring was applied when needed to induce transition.

Drag vs Reynolds number for both spinning and nonspinning models at zero angle of attack is shown in Fig. 2. As noted above, spinning seems to cause premature transition to turbulent-boundary-layer flow in agreement with the pictorial data of Martin.[11]

Testing Procedure

The magnetic balance equipment was turned on and permitted to stabilize with the model suspended for at least 15 min; then the ambient air temperature and presssure were recorded and the model position was adjusted to the desired location and angle of attack as measured by the position transits. The laser position control system was then engaged to hold the set angles of pitch and yaw. When drift in drag, lift, and sideslip position were observed through transits, the model was manually restored to its proper position.

Wind-off-tare balance currents were then recorded. The desired wind speed was set using the micromanometer. A wind-on, zero-spin-tare was recorded. The model was spun using the roll field. When the spin rate, which was monitored on a separate electronic counter, reached its maximum (150-200 rps, depending on wind speed, angle of attack, and boundary-layer trip condition), the roll field was shut off, allowing the spin to decay while the model position was held fixed. The data were recorded at 8-s intervals.

All data were reduced in the IBM 370 at the MIT Information Processing Center using the Magnus Data Reduction Computer Program.[3] In this program the tare side-force current at zero spin was subtracted out for each run, a method used by Platou[12] to correct for slight initial

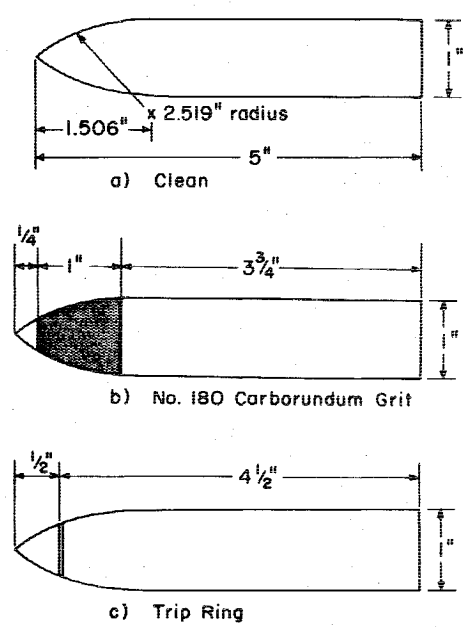

Fig. 1 Model geometry and boundary-layer trip configuration.

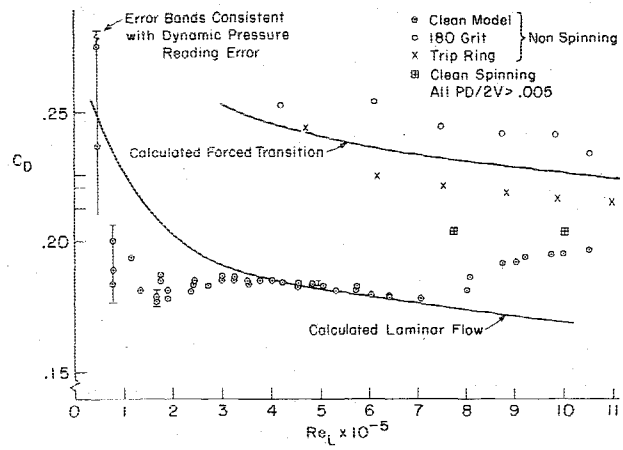

Fig. 2 Drag coefficient vs Reynolds number.

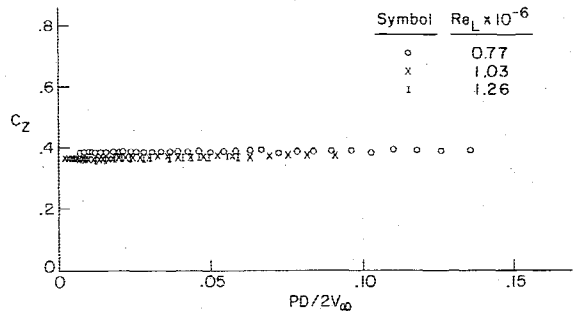

Fig. 3 Normal force coefficient vs $PD/2V_\infty$, $\alpha = 10$ deg.

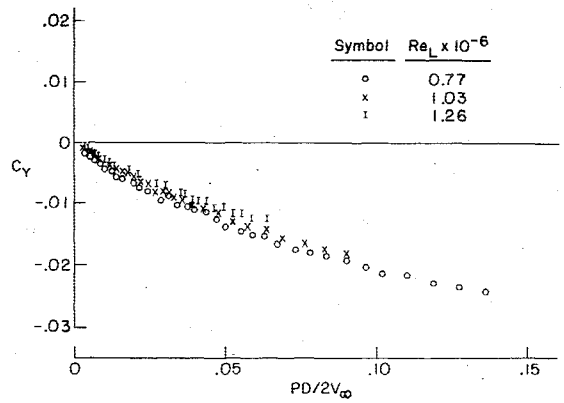

Fig. 4a Side-force coefficient vs $PD/2V_\infty$, $\alpha = 10$ deg.

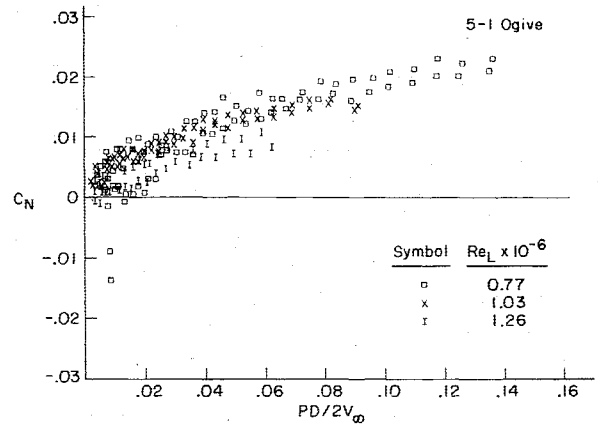

Fig. 4b Yawing-moment coefficient vs $PD/2V_\infty$, $\alpha = 10$ deg.

misalignment in yaw. The slight uncertainty ± 0.15 deg in setting zero angle of attack (during a run, angles of pitch and yaw were held to set values by the laser system within ± 0.02 deg) was resolved, using the averaged C_L values for that run to define a lift curve slope. The angle of attack in the range $|\alpha| < 4$ deg was corrected to be consistent with the lift data. Above 4 deg, the angles reported are those observed using the transits.

Test Results

The results presented here include three series of experimental runs. Initial Magnus measurements were made using the bare ogive-cylinder at small angles of attack. Subsequently, tests in the presence of a sting and with a turbulent boundary layer were made.

During the initial testing period Magnus forces were measured on the bare model for spin rates up to 200 rps, at angles of attack from -5.1 to 10 deg, and at three wind speeds ranging 300-460 ft/s. Subsequent Magnus testing for the effect of stings and boundary-layer trips was carried out at 300 ft/s, as this was where the fullest extent of Magnus reversal was observed. In the final test series, the boundary layer-tripped model was run at 400 ft/s ($Re \simeq 10^6$) to explore the changes caused by further increase in Reynolds number.

Measured Force and Moment Data

Force and moment data were reduced to standard nondimensional coefficients. Figure 3 shows that the normal force coefficient (like the axial force coefficient) is weakly dependent on model spin and length Reynolds number. The measured side force and yawing moment coefficients C_Y and C_N on a smooth model at an angle of attack of 10 deg for three Reynolds numbers are shown as a function of nondimensional spin rate in Figs. 4a and 4b. Similar data at an angle of attack of 2.5 deg are shown in Fig. 5a and b. A detailed examination of Figs. 4 and 5 indicates that the Magnus force coefficient is generally nonlinear at low spin and is not strongly dependent on Reynolds number at the highest angle of attack.

The force and moment data suggest that the center of pressure is essentially fixed, whether in the traditional or reversed Magnus force region. The summary plots, C_Y vs $PD/2V$ curves, from additional runs with a smooth sting free model are given in Figs. 6a and b. These curves at $Re = 0.77 \times 10^6$ show that the reverse Magnus force is very large at small angles of attack. It changes sign at approximately 5 deg and then has the classical (negative) sign at higher angles of attack. Although the Magnus force is strongly spin dependent, the spin rate has little effect on the lift data (Fig. 3).

The positive or reversed value of Magnus force and moment coefficient was an unexpected result. Thus, some additional tests were conducted to determine the validity of the data. Two hypotheses were suggested. First, the reverse loop might be eliminated with a dummy sting. Second, it might be eliminated with a fully turbulent boundary layer, or perhaps with both. The use of a sting required a support rig. The geometry of this equipment is shown in Fig. 7. The effect of the sting holder (with no sting) on C_Y is shown in Fig. 8. The sting holder appears to have no measurable effect on C_Y.

Dummy stings in the sting holder do affect the Magnus side force and moment. This is shown at $Re = 0.77 \times 10^6$ as a function of spin rate in Fig. 9. The effect of the sting is to decrease the reverse Magnus force encountered at low spin rates. The cross plot vs angle of attack at constant spin is shown in Fig. 10 for no sting and 0.25-caliber-diam and 0.50-caliber diam stings. This clearly shows the effect of increasing sting diameter, which decreases the reverse Magnus force.

The effect of a synthetic turbulent boundary layer with no dummy sting can be seen by comparing the data in Figs. 6 and 11 at $Re = 0.77 \times 10^6$. By cross plotting the same data vs angle of attack at constant spin (Fig. 12), it becomes apparent that

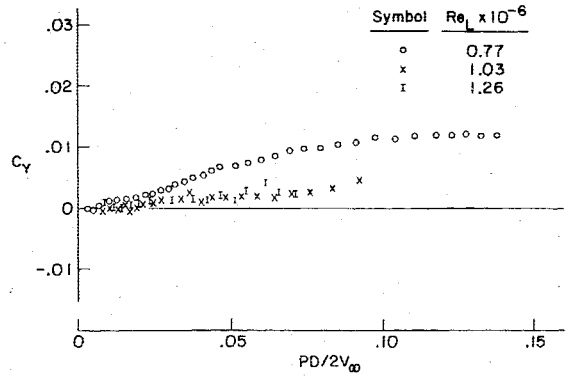

Fig. 5a Side-force coefficient vs $PD/2V_\infty$, $\alpha = 2.53$ deg.

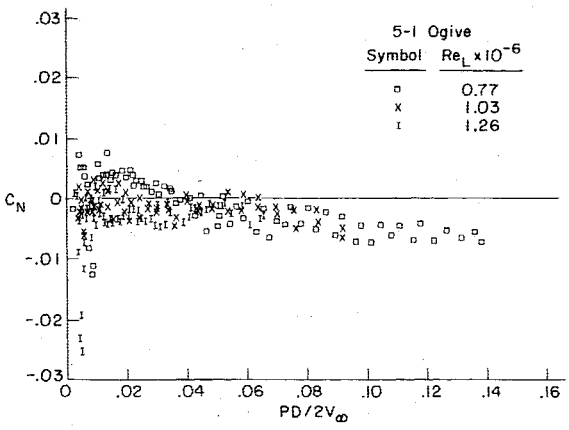

Fig. 5b Yawing-moment coefficient, $\alpha = 2.53$ deg.

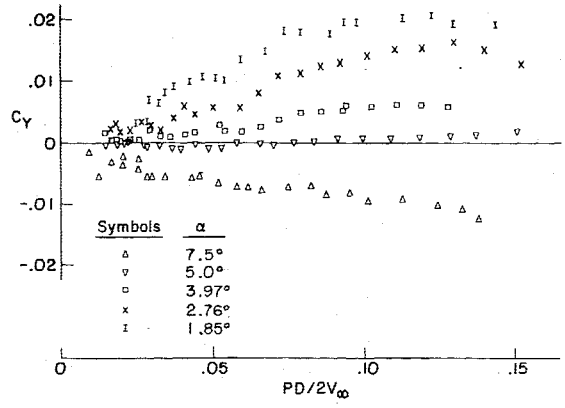

Fig. 6a Bare model side-force coefficient vs $PD/2V_\infty$ at $Re_L = 0.77 \times 10^6$, 7.5 deg $\geq \alpha \geq$ 1.85 deg.

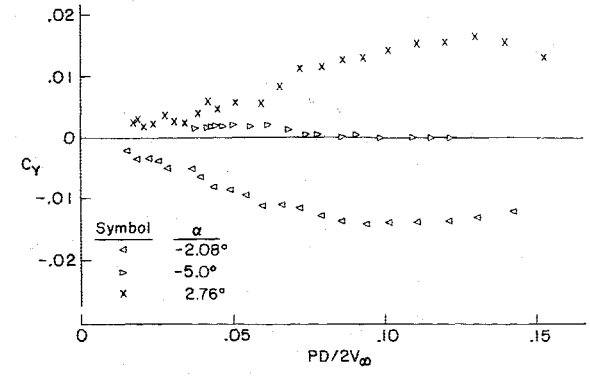

Fig. 6b Bare model side-force coefficient vs $PD/2V_\infty$ at $Re_L = 0.77 \times 10^6$, 2.76 deg $\geq \alpha \geq -5$ deg.

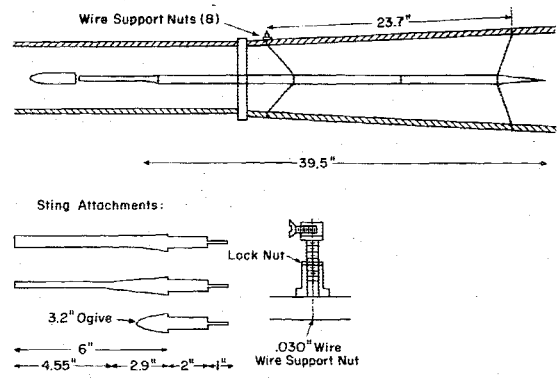

Fig. 7 Magnetic balance dummy sting assembly.

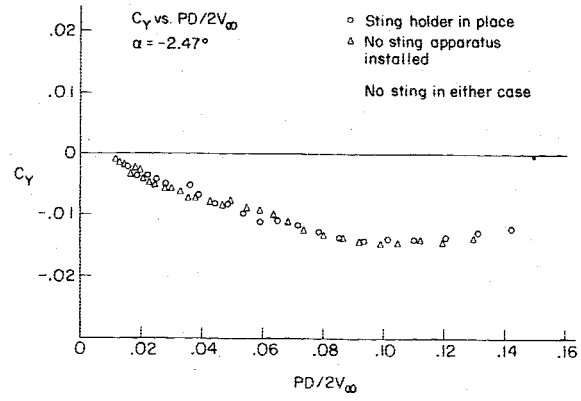

Fig. 8 Sting holder effect 5 – 1 ogive cylinder with no sting.

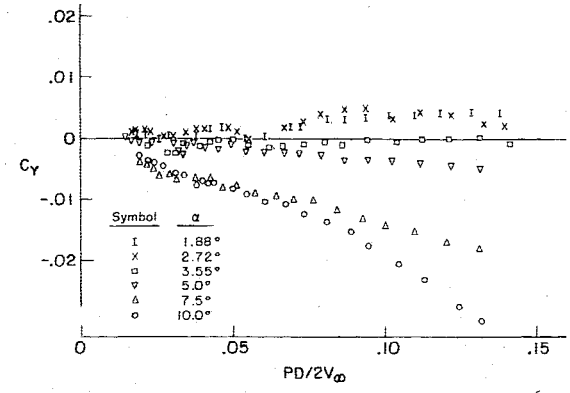

Fig. 9 Side-force coefficient vs $PD/2V_\infty$ at $Re_L = 0.77 \times 10^6$, model with 0.50 caliber sting.

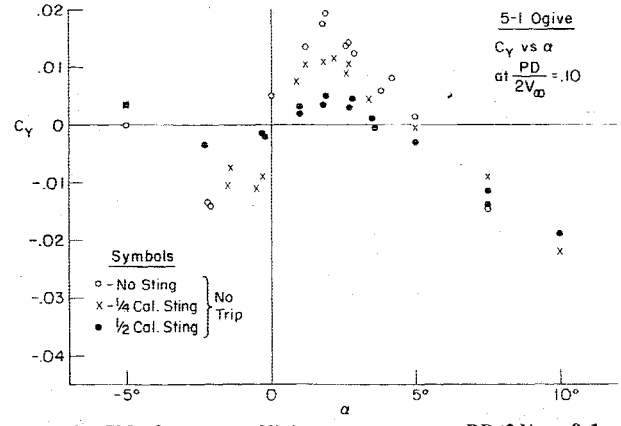

Fig. 10 Side-force coefficient vs α at $PD/2V_\infty = 0.1$ at $Re_L = 0.77 \times 10^6$ showing sting effect.

Table 1 Comparison of experimental data

Source	C_{Z_α}	C_{M_α}	X_{CP}/D[a]	Re	M	Moment reference
Greene	0.040	0.092	—	3.6×10^7	0.23	c.g. (unknown)
Platou	0.042	−0.0512	1.6	3×10^6	0.11	nose
Present data	0.041	−0.065	1.7	0.77×10^6	0.27	nose

[a] Converted to a reference length of 1 diam.

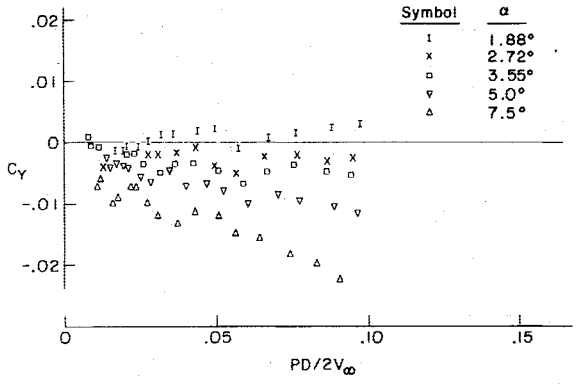

Fig. 11 Side-force coefficient vs $PD/2V_\infty$ at $Re_L = 0.77 \times 10^6$ with artificial transition.

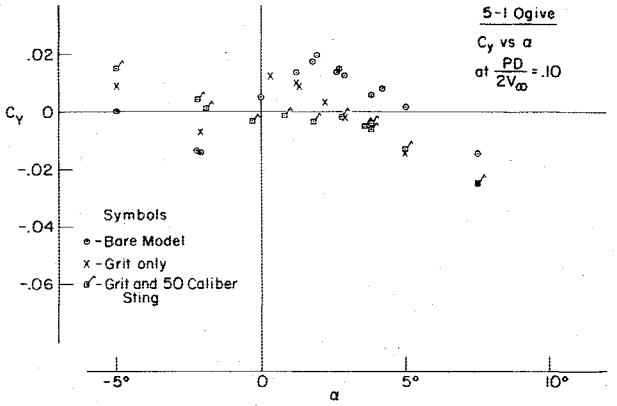

Fig. 12 Side-force coefficient vs α at $PD/2V_\infty = 0.1$ at $Re_L = 0.77 \times 10^6$ showing effect of forced transition.

the reverse region is reduced by adding grit. When the dummy sting was installed behind a grit-roughened model, the reverse Magnus force was almost eliminated at small angles. At the highest Reynolds number tested (10^6), the sting and no-sting data show the same trend as at $Re = 0.77 \times 10^6$.

Comparison with Other Measurements

The amount of other data with which these data can be compared is limited. The comparison data fall into two classes. The most important is that of Martin and Ingram.[11] These data show the same reverse Magnus force for a fineness ratio 7 body with a turbulent layer. Only Magnus data are given. Carmen et al.[13] presented only Magnus forces for a 5-caliber body. Greene[14] and Platou[15] present relatively complete data for 5-caliber bodies. The first comparison shows the slope of the normal force coefficient curve and the slope of the pitching moment coefficient curve near zero angle of attack (Table 1). The general agreement shown is acceptable for normal force and center of pressure. The difference of 0.1 diam on the center of pressure is at the limit of error for the data taken here (±0.1 diam). Platou's error bands are not listed. As explained below, the error in C_Z is about ±0.002 in the data obtained in the magnetic balance.

Data from Platou's report[15] are presented in Fig. 13. It shows a curve of C_{NP}, the Magnus force parameter, plotted against angle of attack. The filled symbols are data taken from Greene,[14] and the open symbols represent Platou's data. The center of pressure from each investigator is in good agreement, whereas the size of the Magnus force coefficient, as determined by Greene, is about 0.1 times that determined by Platou.

Correcting Greene's data for the difference in Reynolds number of a factor of 10 using[2]

$$C_{N_P} \propto 1/\sqrt{Re} \tag{1}$$

still leaves it a factor of three lower than Platou's.

Table 2 Magnus side force coefficient at a reduced spin of 0.045

α	C_Y[11]	C_Y[15]	C_Y present data[16]
2.5	0.0112	−0.0013	0.0065
5	0.0110	−0.0031	0
7.5	0.0045	−0.0077	−0.008
10	−0.0045	−0.0122	−0.013

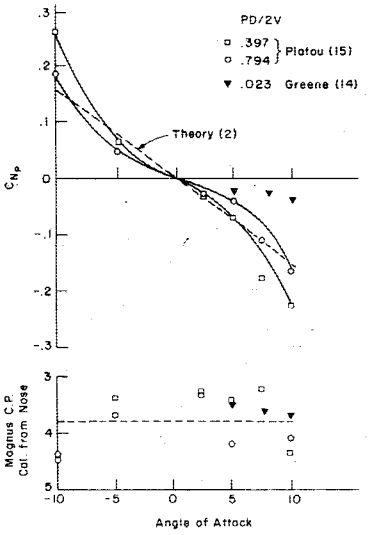

Fig. 13 Magnus force on the five-caliber tangent ogive after Platou.[12]

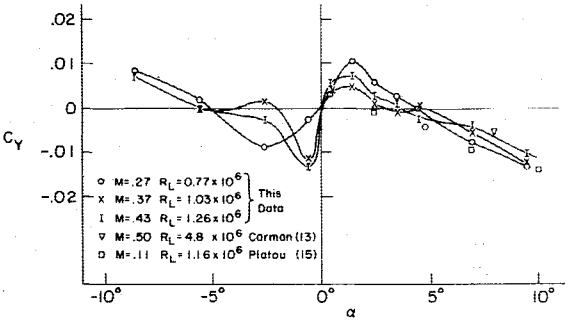

Fig. 14 Side-force coefficient vs α at $PD/2V_\infty = 0.0450$ (fineness ratio 5).

Figure 14 shows the measured Magnus force coefficient plotted at a reduced spin of 0.045. It was assumed in calculating these values that both Martin and Platou's C_{NP} could be linearly converted. Thus, Platou's values at $PD/2V$ of (0.4) were corrected to the value used here (0.045). The results are given in Table 2. The fineness-ratio difference between Martin ($L/D=7$) and Platou ($L/D=5$) would tend to cause the Magnus effect to be enhanced.

Except for the reversed loop, Platou's data[15] for $Re=1.15\times10^6$ are in fair agreement with the present data at $Re=0.77\times10^6$. Difference in tunnel turbulence levels could easily account for this.

Error Analysis

A detailed review of the data indicates that

$\Delta C_X \simeq \pm 0.002$ $\quad$ $\Delta C_M \simeq \pm 0.015$
$\Delta C_Y \simeq \pm 0.003$ $\quad$ $\Delta C_N \simeq \pm 0.020$
$\Delta C_Z \simeq \pm 0.002$ $\quad$ $\Delta\alpha \simeq \pm 0.015$ deg within a run
± 0.15 from run to run

Discussion

The data presented indicate that in the Reynolds number range 0.7×10^5-1.0×10^6, a reverse Magnus force occurs at small angle of attack. The magnitude of the effect is larger at a fixed reduced spin ($PD/2V_\infty$) as the Reynolds number is lower. This Reynolds-number sensitivity becomes smaller at higher angles of attack. The presence of dummy support stings and boundary-layer trips can virtually eliminate this reverse Magnus region. When there is no sting, the Magnus force coefficient on the model with forced transition is about the same size as that measured on a smooth model if the angle of attack is reasonably high (Figs. 6 and 11).

The forced transition case should result in a nearly axially symmetric transition locus. However, Sturek's data[17-19] show that this is not the case with natural transition. No further comments can be made since the comparison was not studied.

The experimental results presented here confirm existence of the reverse spin Magnus force at low angles of attack and low spin rates. Further data presented here show the phenomenon exists for a fineness ratio five bodies while other data were for a fineness ratio seven bodies.[11] Martin and Ingram have not discussed support interference, which is shown here to be large in some circumstances. Hence, generalizations to other fineness ratios must be made with care.

At present no linear approximation (see Ref. 20 for a discussion of linear approximations) can account for detailed changes in the flow pattern to produce the following observed facts: 1) The weak fractional increase in normal force due to spin; 2) The change in direction of the Magnus force, without a large change in the center of pressure location (at least for the conditions of these tests); 3) The marked upstream influence of the sting for a fineness ratio of five bodies.

The data suggest the center of pressure is well behaved, even in the presence of the unexpected upstream influence of the sting. The cross-force coefficient $(C_Z^2+C_Y^2)^{1/2}$ increases slightly with spin rate.

Acknowledgment

This research was supported under Contract DAAD05-74-C-0735 by the U.S. Army, Ballistic Research Laboratories, Aberdeen Proving Ground, Md., and under Contract DAHC04-75-C-0001 by the U.S. Army Research Office, Durham, North Carolina.

References

[1]Fletcher, C. A. J., "Negative Magnus Forces in the Critical Reynolds Number Regime," *Journal of Aircraft*, Vol. 9, Dec. 1972, pp. 826-833.

[2]Martin, J. C., "On Magnus Effects caused by Boundary Layer Displacement Thickness on Bodies of Revolution at Small Angles of Attack," BRL Report 870, U.S. Army Ballistic Research Laboratories, Aberdeen Proving Ground, Md., June 1975.

[3]Birtwell, E. P., "Magnus Forces and Sting Interference on Magnetically-Suspended Ogive Cylinders," S.M. Thesis, Department of Aeronautics and Astronautics, MIT, Cambridge, Mass., May 1974.

[4]Krahn, E., "Negative Magnus Force," *Journal of The Aeronautical Sciences*, Vol. 23, April 1956, p. 377.

[5]Swanson, W. M., "Magnus Effect: A Summary of Investigations to Date," *Journal of Basic Engineering*, Vol. 83, Sept. 1961, pp. 461-470.

[6]Vlajinac, M., "Design, Construction and Evaluation of a Subsonic Wind Tunnel," S.M. Thesis, Department of Aeronautics and Astronautics, MIT, Cambridge, Mass., June 1970.

[7]Vlajinac, M. and Covert, E. E., "Sting-Free Measurements of Sphere Drag in Laminar Flow," *Journal of Fluid Mechanics*, Vol. 54, Part 3, Aug. 1972, pp. 385-392.

[8]Covert, E. E., Vlajinac, M., Stephens, T., and Finston, M., "Magnetic Suspension and Balance Systems for Wind Tunnel Use," *Progress in Aerospace Sciences*, Vol. 14, Pergamon, London, 1973.

[9]Judd, M., Vlajinac, M., and Covert, E. E., "Sting-Free Drag Measurements on Ellipsoidal Cylinders at Transition Reynolds Numbers," *Journal of Fluid Mechanics*, Vol. 48, Part 2, July 1971, pp. 353-364.

[10]Gilliam, G. D., "Data Reduction Techniques for Use with a Wind Tunnel Magnetic Suspension and Balance System," NASA CR-111844, June 1970; also MIT Aerophysics Laboratory Rept. No. 167.

[11]Martin, J. M. and Ingram, C. W., "Experimental Correlation between the Flow and Magnus Characteristics of a Spinning Ogive-Nose Cylinder," *AIAA Journal*, Vol. 11, July 1973, pp. 901-902.

[12]Platou, A. S., "Wind Tunnel Magnus Testing of a Canted Fin of Self-Rotating Configuration," *AIAA Journal*, Vol. 10, July 1972, pp. 965-967.

[13]Carman, J. B., Uselton, J. C., and Summers, W. E., "Experimental Magnus Characteristics of Basic and Boattail Configurations of 3- and 5-Caliber Army-Navy Spinner Projectiles at Subsonic and Transonic Mach Numbers," AEDC-TR-70-36, April 1970.

[14]Greene, J. E., "A Summary of Experimental Magnus Characteristics of a 7- and 5-Caliber Body of Revolution at Subsonic through Supersonic Speeds," U.S. Naval Ordnance Laboratory, White Oak, Md., NAVORD, Report 6110, Aug. 1958.

[15]Platou, A. S., Edgewood Arsenal Magnus Tests, Unpublished, Ballistic Research Laboratory, Memorandum, AMXRD-BEL, U. S. Army Aberdeen Proving Ground, Md., April 1971.

[16]Birtwell, E. P., Coffin, J. B., Covert, E. E., and Haldeman, C. W., "Some Measurements of the Magnus Characteristics on a Magnetically-Suspended 5-Caliber Ogive Cylinder," MIT Aerophysics Laboratory Rept. TR 193, July 1976, BRL Rept. CR 328. Note: numerous errors in this report have been corrected in the present material.

[17]Sturek, W. B., "Boundary Layer Studies on Spinning Bodies of Revolution," BRL Memorandum Rept. 2381, Aberdeen Proving Ground, Md., May 1974.

[18]Sturek, W. B., "Boundary Layer Studies on Spinning Tangent-Ogive-Cylinder Models," BRL Rept. 1801, Aberdeen Proving Ground, Md., July 1975.

[19]Sturek, W. B., "Preliminary Surveys of the Three-Dimensional Boundary Layer on a Yawed, Spinning Body of Revolution," BRL Memorandum Rept. 2501, Aberdeen Proving Ground, Md., July 1975.

[20]Ashley, H. and Landahl, M., *Aerodynamics of Wings and Bodies*, Addison-Wesley, Reading, Mass., 1965, Chapt. 6.7 for a discussion of the "Slender Body Approximation."